Respective influences of IOD and ENSO on the Tibetan snow cover in early winter

Chaoxia Yuan · Tomoki Tozuka · Takafumi Miyasaka ·
Toshio Yamagata

Abstract Using reanalysis data and snow cover data derived from satellite observations, respective influences of Indian Ocean Dipole (IOD) and El Niño/Southern Oscillation (ENSO) on the Tibetan snow cover in early winter are investigated. It is found that the snow cover shows a significant positive partial correlation with IOD. In the pure positive IOD years with no co-occurrences of El Niño, negative geopotential height anomalies north of India are associated with warm and humid southwesterlies to enter the plateau from the Bay of Bengal after rounding cyclonically and supply more moisture. This leads to more precipitation, more snow cover, and resultant lower surface temperature over the plateau. These negative geopotential height anomalies north of India are related to the equivalent barotropic stationary Rossby waves in the South Asian wave guide. The waves can be generated by the IOD-related convection anomalies over the western/central Indian Ocean. In contrast, in the pure El Niño years with no co-occurrences of the positive IOD, the anomalies of moisture supply and surface temperature over the plateau are insignificant, suggesting negligible influences of ENSO on the early winter Tibetan snow cover. Further analyses show that ENSO is irrelevant to the spring/early summer Tibetan snow cover either, whereas the IOD-induced snow cover anomalies can persist long from the early winter to the subsequent early summer.

Keywords Tibetan snow cover · Indian Ocean Dipole · El Niño/Southern Oscillation · Wave-activity flux

C. Yuan (✉) · T. Tozuka · T. Miyasaka · T. Yamagata
Department of Earth and Planetary Science,
Graduate School of Science, The University of Tokyo,
7-3-1 Hongo, Bunkyo-ku, Tokyo 113-0033, Japan
e-mail: yuan@eps.s.u-tokyo.ac.jp

1 Introduction

Since Blanford (1884) first hypothesized a negative correlation between the wintertime snow accumulation over the Himalayas and the summertime monsoon precipitation over the western India in his seminal paper, many studies have been devoted to impacts of the Himalayan/Tibetan snow on the global climate (see Yamagata and Masumoto 1989). It has been claimed that the excessive snow accumulation in winter lowers not only the wintertime ground temperature by reflecting more incoming solar radiation but also the ground temperature in the subsequent spring and early summer through hydrological processes; a large portion of the available solar energy is used to melt the excessive snow and to evaporate the water rather than to heat the ground (Shukla 1984; Shukla and Mooley 1987). This anomalously low ground temperature over the plateau in the early summer reduces the land-sea thermal gradient, and thus postpones the onset of the Indian summer monsoon. The prolonged influence even weakens the strength of the Indian summer monsoon (Walker 1910; Hahn and Shukla 1976; Kripalani et al. 2003; Fasullo 2004). It also cools the overlying atmosphere in the mid-troposphere and induces a westward extension of the subtropical high in the western Pacific, which is an important constituent of the East Asian summer monsoon system. The consequence is the modification of the monsoonal wind path (Wu and Qian 2003; Zhang et al. 2004). Thus, more summer precipitation is observed from the middle reaches of the Yangtze River valley in China to Japan, whereas less summer precipitation is observed in the southern and southwestern China, and the southeastern Asia.

Above studies, however, do not discuss detailed mechanisms that generate annual snow anomalies over

the plateau. For this reason, Shaman and Tziperman (2005) investigated the role of El Niño/Southern Oscillation (ENSO). The winter sea surface temperature anomalies (SSTA) associated with ENSO in the tropical Pacific excite the stationary Rossby waves that extend along the North African–Asian jet. This modifies the winter storm activities and snowfall over the plateau. However, no study to date has investigated the influences of SSTA in the Indian Ocean even though the moisture supply for the precipitation over the plateau mainly originates from the northern Indian Ocean (both the Arabian Sea and the Bay of Bengal). One of the major causes of the interannual SST variability during the boreal fall and early winter in the tropical Indian Ocean is the Indian Ocean Dipole (IOD) (Saji et al. 1999; Yamagata et al. 2004). Therefore, it is interesting to investigate influences of IOD on the snow cover over the plateau. Since IOD generally ends during the boreal winter and the mid-tropospheric trough above the Indian peninsula is dramatically weakened at around the end of October (Fig. 1), we just focus on the influences of IOD on the Tibetan snow cover (TSC) during November and December (early winter). In these months, TSC develops rapidly and shows a very large interannual variability (Li 1993; Qin et al. 2006). We also discuss the influences of ENSO on TSC in early winter. Since ENSO and IOD sometimes co-occur, it is important to identify their respective influences on TSC.

2 Data and methods

We use recently released snow cover data from the National Oceanic and Atmospheric Administration (NOAA)/ National Environmental Satellite, Data and Information Service (NESDIS), which is available at http://www.cpc.ncep.noaa.gov/data/snow/. The data consists of digitized weekly charts of snow cover derived from visual interpretation of the advanced very high resolution radiometer (AVHRR) geostationary operational environmental satellite (GOES), and other visible-band satellite data. The charts are digitized weekly on an 89×89 polar stereographic grid for the Northern Hemisphere with cell resolutions ranging from 16,000 to 42,000 km^2 and have binary values; 1 for a cell at least 50% covered by snow and 0 not. The dataset used in the study has been regridded on a $2° \times 2°$ grid and covers a period from January 1973 to December 1999 to avoid incompleteness before 1973 and possible inconsistency after 1999 due to the start of a new snow cover product. Monthly HADISST (Rayner et al. 2003) and NECP/NCAR reanalysis (Kalnay et al. 1996) datasets are also used for a period from January 1951 to December 1999. ECMWF ERA-40 dataset obtained from the ECMWF data server from September 1957 to December 1999 is used to compare with NCEP/NCAR data in our composite analyses.

Since the snow cover data is weekly and binary, the early winter snow cover percentage (EWSCP) is defined in the present study as percentage of weeks covered by snow from

Fig. 1 Climatological geopotential height (m) at 500 hPa from September to December based on the NCEP/ NCAR reanalysis data from 1951 to 1999
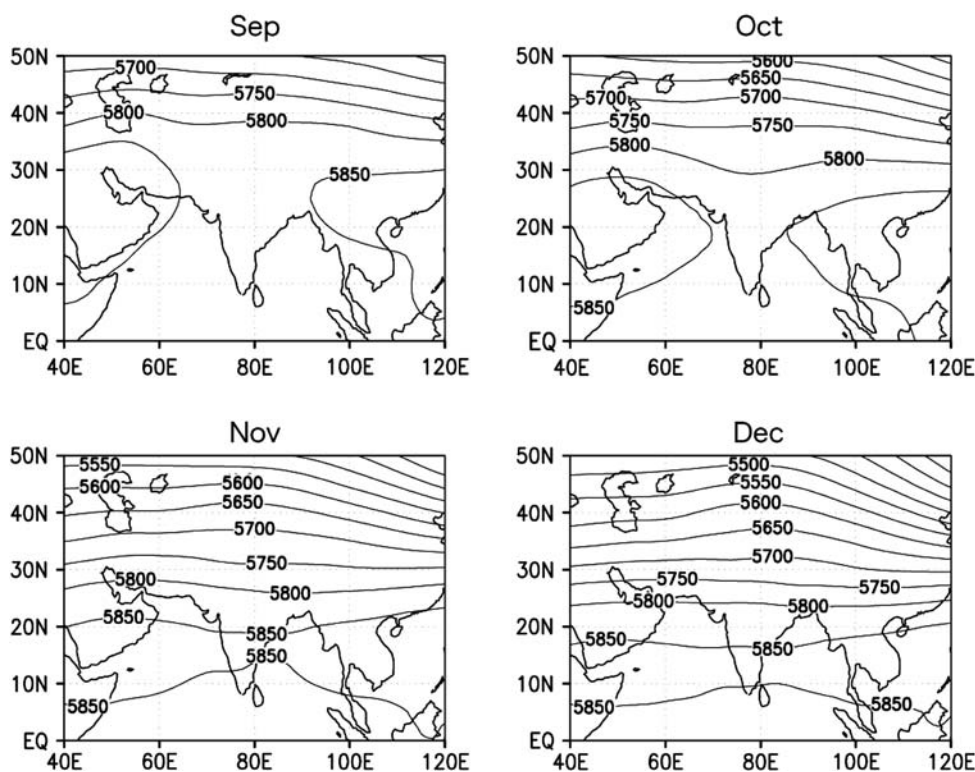
November to December to reflect snow cover variation. The Dipole Mode Index (DMI) is defined as the peak time (September–November) SSTA differences between its western (40°–60°E, 10°S–10°N) and eastern (90°–110°E, 10°S-Equator) poles. We note here that we have shifted the domain of the western pole by 10° in this paper to obtain clearer views. However, conclusions are basically the same if we adopt a conventional definition of DMI. The ENSO index is also the peak time (November–January) Niño-3 (90°–150°W, 5°S–5°N) SSTA.

Since IOD and ENSO sometimes co-occur, we use a partial correlation analysis to extract a sole influence of IOD or ENSO on the early winter TSC. It is calculated by

$$r_{13,2} = (r_{13} - r_{12} \cdot r_{23})/\sqrt{(1-r_{12}^2)(1-r_{23}^2)}, \quad (1)$$

where $r_{13,2}$ is the partial correlation between variable 1 and variable 3 without influences from variable 2 and r_{13}, r_{12}, and r_{23} are correlation coefficients. All time series used for the partial correlation analysis in this study are linearly detrended.

To show the impacts of IOD/ENSO on the moisture budget over the plateau, the moisture flux is calculated by

$$Q_u = \frac{1}{g}\int_{P_{top}}^{P_{surf}} qu\,dP, \quad Q_v = \frac{1}{g}\int_{P_{top}}^{P_{surf}} qv\,dP, \quad (2)$$

where P is pressure, P_{surf} is the surface pressure, P_{top} is the pressure of the top moisture layer (300 hPa in NCEP/NCAR data and 1 hPa in ECMWF data), q is the specific humidity, and (u, v) are horizontal velocity components.

A wave-activity flux $\vec{W}$ of wave-activity pseudo-momentum derived by Takaya and Nakamura (2001) is also used to reveal possible mechanisms connecting IOD and ENSO with TSC. The flux, parallel to the local three-dimensional group velocity in the WKB limit, can be used to diagnose generation, propagation, and absorption of quasi-geostrophic wave-packets on a zonally varying basic flow. Its form in a stationary wave field in the spherical co-ordinate is

zonal and meridional directions, $|\vec{U}|$ is the magnitude of the winds, f_0 is the Coriolis parameter, and N^2 is the buoyancy frequency. Readers are referred to Takaya and Nakamura (2001) for more details.

3 Early winter snow cover

Figure 2 shows the spatial distribution of the mean EWSCP and its standard deviation for the period from 1973 to 1999. A high percentage is seen in high latitudes and mountainous regions; the percentage over 90% covers most of the continent north of 50°N. Locations of the high standard deviation are seen along the snow line close to the largest gradient of EWSCP crossing the continent zonally. We note that the Tibetan Plateau, due to its high altitude, differs from other parts at the same latitude because of the existence of snow cover in early winter. It even shows the highest standard deviation. The results of snow cover based on the satellite data compare well with those based on the observed Soviet snow depth data (Kripalani and Kulkarni 1999).

The seasonal cycle of the snow cover percentage (mean percentage of weeks covered by snow in a month) is also calculated and averaged over the plateau (75°–100°E; 25°–40°N) from January 1973 to December 1999. Figure 3 shows that the snow cover starts to build up in September, increases significantly during the early winter, peaks in January, and starts to decay thereafter. The correlation coefficient between the early winter (November–December) snow cover and the whole winter (November–February) snow cover is 0.83. This indicates that the interannual variability of snow cover in the whole winter can be mostly explained by that in the early winter. Therefore, examining causes of the snow cover variability in the early winter is important to understand the whole winter snow cover variability over the plateau.

$$\vec{W} = \frac{p\cos\phi}{2|\vec{U}|}\begin{pmatrix} \dfrac{U}{a^2\cos^2\phi}\left[\left(\dfrac{\partial\psi}{\partial\lambda}\right)^2 - \psi\dfrac{\partial^2\psi}{\partial\lambda^2}\right] + \dfrac{V}{a^2\cos\phi}\left[\dfrac{\partial\psi}{\partial\lambda}\dfrac{\partial\psi}{\partial\phi} - \psi\dfrac{\partial^2\psi}{\partial\lambda\partial\phi}\right] \\[2ex] \dfrac{U}{a^2\cos\phi}\left[\dfrac{\partial\psi}{\partial\lambda}\dfrac{\partial\psi}{\partial\phi} - \psi\dfrac{\partial^2\psi}{\partial\lambda\partial\phi}\right] + \dfrac{V}{a^2}\left[\left(\dfrac{\partial\psi}{\partial\phi}\right)^2 - \psi\dfrac{\partial^2\psi}{\partial\phi^2}\right] \\[2ex] \dfrac{f_0^2}{N^2}\left\{\dfrac{U}{a\cos\phi}\left[\dfrac{\partial\psi}{\partial\lambda}\dfrac{\partial\psi}{\partial z} - \psi\dfrac{\partial^2\psi}{\partial\lambda\partial z}\right] + \dfrac{V}{a}\left[\dfrac{\partial\psi}{\partial\phi}\dfrac{\partial\psi}{\partial z} - \psi\dfrac{\partial^2\psi}{\partial\phi\partial z}\right]\right\} \end{pmatrix}. \quad (3)$$

Here (λ, ϕ) are longitude and latitude, a is the Earth's radius, $z = -H \ln p$, $p = $ pressure/1,000 hPa, H is the constant scale height, ψ is the perturbation of geostrophic streamfunction, (U, V) are the climatological winds in the

3.1 Correlation analysis

The spatial distribution of correlation coefficients between DMI (Niño-3) and EWSCP from 1973 to 1999 is shown in
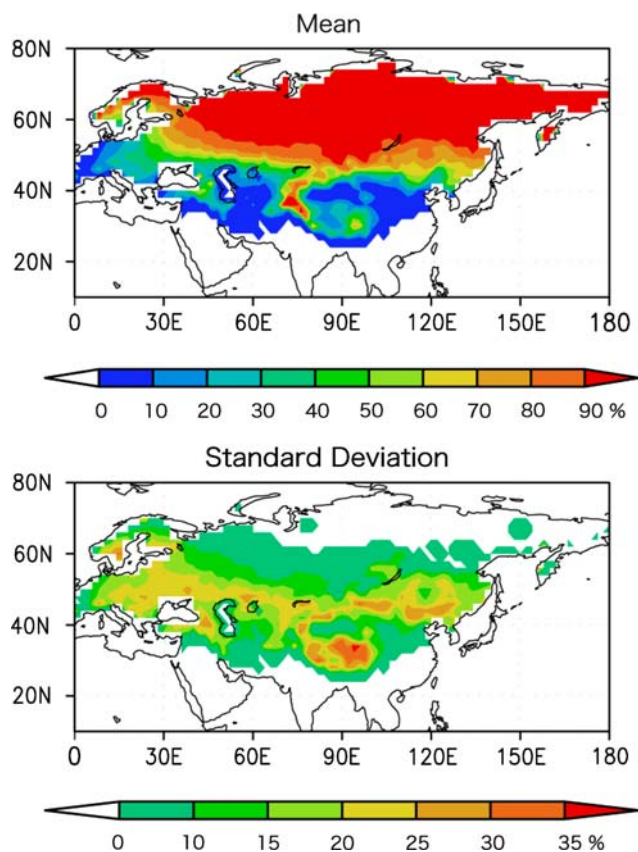
Fig. 2 November–December snow cover percentage (*upper panel*) and its standard deviation (*lower panel*) over the Eurasian continent for a period from 1973 to 1999
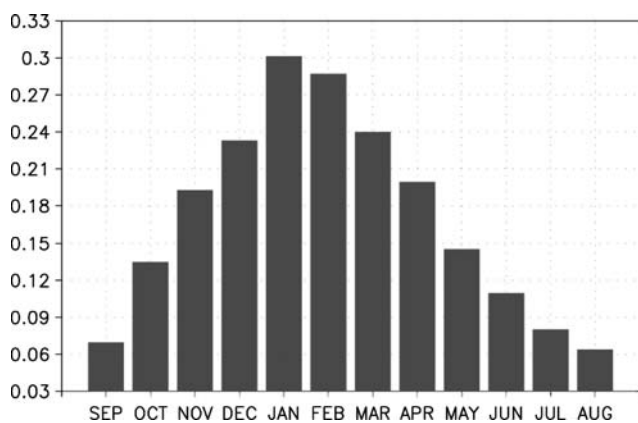

Fig. 3 Seasonal cycle of snow cover ratio averaged over the Tibetan Plateau for a period from January 1973 to December 1999

Fig. 4. After excluding the influences from ENSO, IOD has a statistically significant positive partial correlation with EWSCP over nearly the whole plateau above 3,000 m (Fig. 4a). The positive correlation between IOD and EWSCP remains even in a normal correlation analysis (Fig. 4b). On the other hand, when the influences from IOD are removed, ENSO shows a negative partial correlation

with EWSCP (Fig. 4c). But the negative partial correlation between ENSO and EWSCP almost disappears because of the cancellation effect when the normal correlation is calculated (Fig. 4d).

Figure 5 shows the lead-lag partial correlation coefficients between DMI (dark bar) and the 2-month-mean snow cover percentage averaged over the plateau after excluding the influences of ENSO from the preceding March in the same year to the subsequent July in the second year. It is shown that IOD keeps the statistically significant positive partial correlation with TSC from the early winter (November–December) to the subsequent early summer (May–June). Ferranti and Molteni (1999) suggested that the interannual variability of the Eurasian snow depth in early spring is dependent on the atmospheric circulation patterns during the preceding winter. Kripalani (2007) has shown that winter and spring snow depth over Eurasia is highly correlated. Thus, this prolonged positive partial correlation between DMI and TSC may be due to the persistence of the IOD-related snow anomalies in early winter even if IOD demises near the end of a calendar year.

On the other hand, the partial correlation coefficient between ENSO index and TSC after excluding the influences from IOD (Fig. 5, grey bar) is significantly negative from November to January and becomes insignificant thereafter. This is contrasted with Shaman and Tziperman (2005), who used a 9-year-long snow depth data and showed a positive correlation between ENSO during January-March and the Tibetan snow depth during the subsequent July–September. They claimed that ENSO can cause an increase in snowfall over the plateau in winter and the snow anomalies can persist till the subsequent summer. Since the direct positive atmospheric influence of ENSO on TSC is denied by our analysis, the hypothesis of Shaman and Tziperman (2005) cannot be supported. Instead, we suggest the following scenario. It is now well known that ENSO introduces the basin-wide SSTA in the Indian Ocean mostly through the atmospheric teleconnection (e.g., Yamagata et al. 2004). This oceanic thermal memory may last long till the subsequent summer (Alexander et al. 2004) and influence the moisture transport of the Indian summer monsoon toward the Asian continent, which may lead to an increase in precipitation over the Tibetan Plateau in the subsequent summer. The anomalous precipitation may contribute to the snow depth in the mountainous regions where snow remains with surface temperature below the freezing point even in summer.

3.2 Composite analysis

To examine the results from the partial correlation analysis, composites based on pure IOD (ENSO) years are constructed. Pure IOD (ENSO) years are selected based

Fig. 4 Distribution of normal (*right panels*) and partial (*left panels*) correlation coefficients between DMI and EWSCP (*upper panels*) and between Niño-3 and EWSCP (*lower panels*) for a period from 1973 to 1999. The values of 0.24, 0.32 and 0.44 are at 90, 95 and 99% significance levels by *t* test
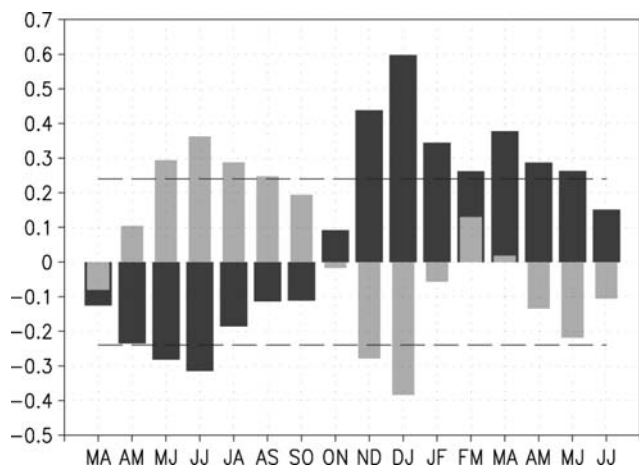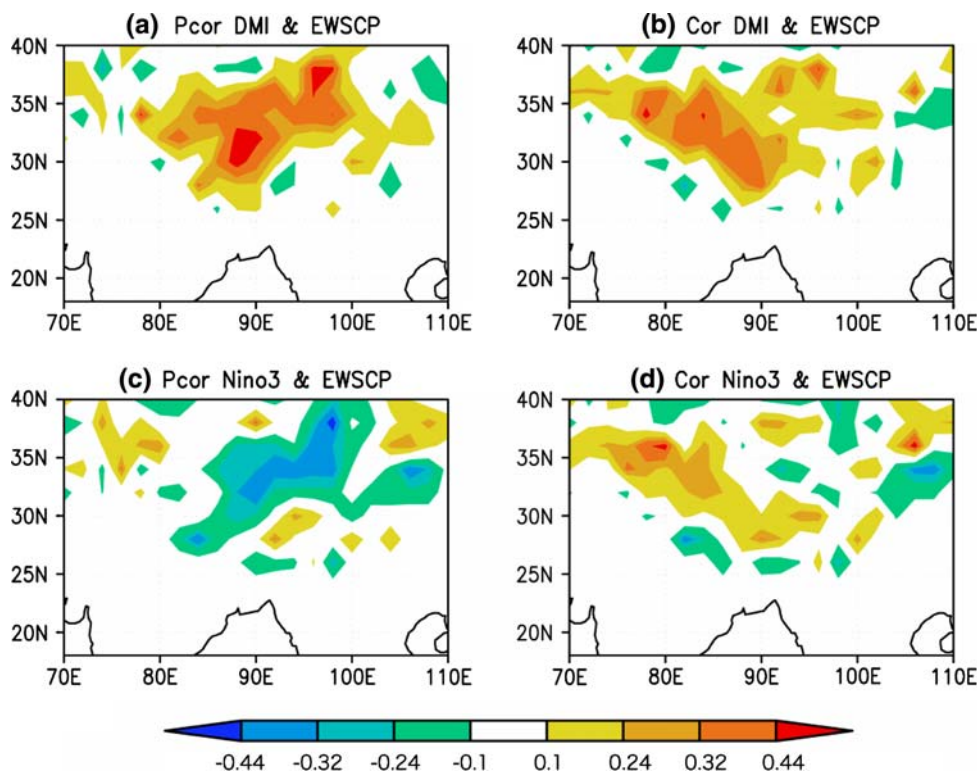

Fig. 5 Lead-lag partial correlation coefficients between DMI (*dark bar*)/Niño-3 index (*grey bar*) and the 2-month-mean snow cover percentage averaged over the Tibetan Plateau from the preceding March of the same year to the subsequent July of the second year for a period from 1973 to 1999. Dashed lines denote the correlation coefficients at a 90% significance level by *t* test

Fig. 6 Normalized time series of DMI (*upper panel*) and Niño-3 (*lower panel*) from 1951 to 1999. Pure IOD and ENSO years are darkened

on the criterion that DMI (Niño-3 index) exceeds 0.8 sigma of standard deviation with Niño-3 index (DMI) within 0.8 sigma. To obtain more pure event years, we use the time series of IOD and ENSO indices from 1951 to 1999 (Fig. 6). Then four positive (1961, 1967, 1977, 1994) and six negative (1958, 1959, 1964, 1980, 1992, 1996) pure IOD years and five pure El Niño (1957, 1965,
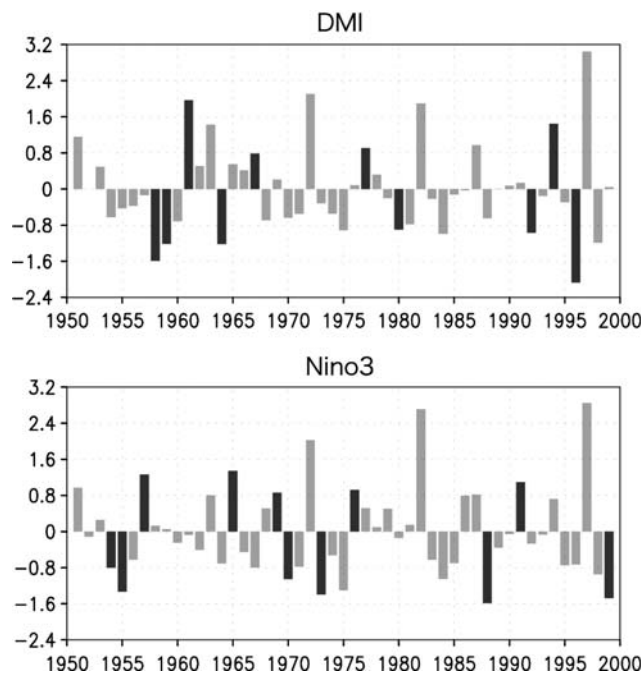
1969, 1976, 1991) and six pure La Niña (1954, 1955, 1970, 1973, 1988, 1999) years are selected. All events in these years are used to make composites based on the

Fig. 7 November–December
anomaly composites of 500 hPa
geopotential height (**a**, **b** in m),
moisture flux (**c**, **d** in
kg m^{-1} s^{-1}), and surface
temperature (**e**, **f** in °C) in pure
positive IOD years based on
NCEP/NCAR (*left panels*) and
ECMWF (*right panels*) data.
Anomalies with significance
levels at 90% by two-tailed
t test are shaded
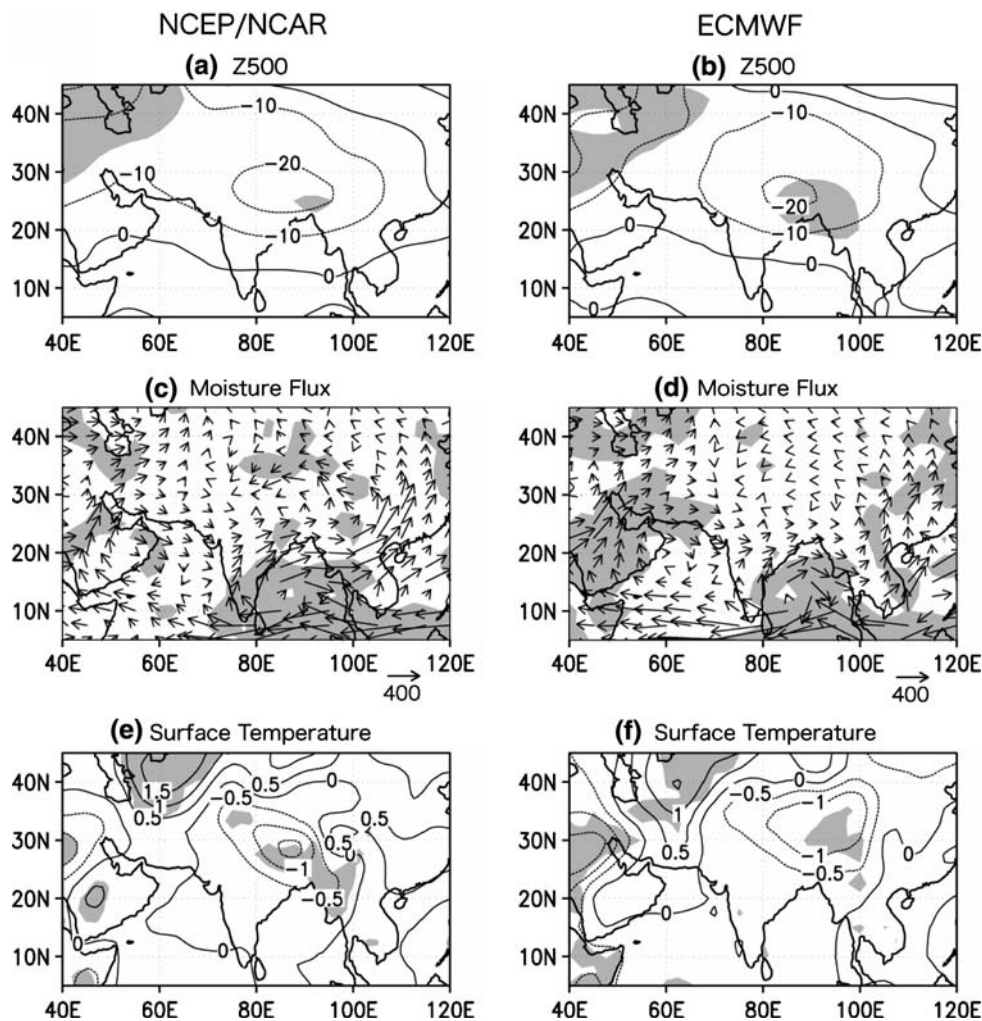
NCEP/NCAR dataset. Because the ECMWF dataset starts from 1957, two pure La Niña years, 1954 and 1955, have to be excluded in the composites based on this dataset. Note that the anomalies for composites are defined as the deviations from mean values during November–December and those at a 90% significance level by the two-tailed *t* test are shaded.
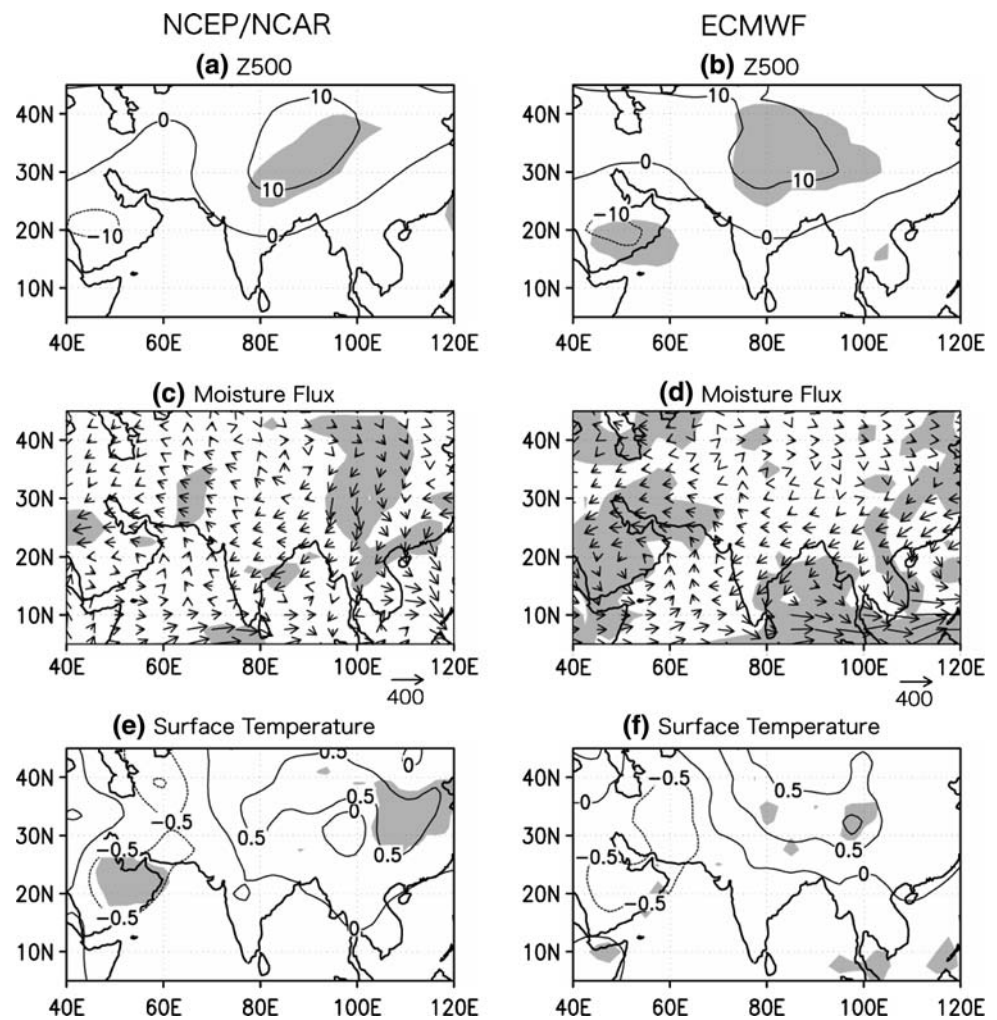
3.2.1 Influences of IOD

We find negative geopotential height anomalies north of India at 500 hPa in the pure positive IOD years (Fig. 7a, b). These circulation anomalies in the mid-troposphere are associated with warm and humid southwesterly anomalies to enter the plateau from the Bay of Bengal after rounding cyclonically and supply more moisture. As shown in Fig. 7c and d, anomalous moisture fluxes direct northeastward from the Bay of Bengal and turn cyclonically toward the plateau. In fact, the moisture budget analysis over the plateau shows the moisture convergence anomaly

of 1.98×10^8 (1.08×10^8) kg s^{-1} based on NCEP/NCAR (ECMWF) data. When these warm and humid airflows from the Bay of Bengal meet the cold and dry northerlies, active convection starts over the plateau and leads to more precipitation and lower surface temperature (Fig. 7e, f). Winter precipitation, even if it is in an aqueous phase, is equivalent to snowfall over the Tibetan Plateau since the surface temperature is below the freezing point. The lower surface temperature is favorable for further snow accumulation and persistence.

In contrast, the geopotential height anomalies north of India at 500 hPa are positive in the pure negative IOD years (Fig. 8a, b), which hinder the access of warm and humid airflows from the northern Indian Ocean to the plateau (Fig. 8c, d). This is why the moisture budget over the plateau shows the divergence anomaly of 2.05×10^8 (0.64×10^8) kg s^{-1} based on the NCEP/NCAR (ECMWF) data. Thus, we find higher surface temperature (Fig. 8e, f), and resultant less snow cover over the plateau in the pure negative IOD years.

3.2.2 Influences of ENSO

In the pure El Niño years, weak positive geopotential height anomalies at 500 hPa can be found from the Bay of Bengal to the northern part of India in the NECP/NCAR data (Fig. 9a). Those are even weaker in the ECMWF data (Fig. 9b). The anomalous moisture flux at around 20°N is significant and mostly eastward from the northern part of India to the southern part of China (Fig. 9c, d). The moisture divergence anomaly over the plateau, however, is 2.3×10^7 (3.3×10^7) kg s^{-1} based on NCEP/NCAR (ECMWF) data, which is much smaller than the value of 2.05×10^8 (0.64×10^8) kg s^{-1} for the pure negative IOD years. The anomalies of surface temperature are not significant over the plateau (Fig. 9e, f).

Pure La Niña years show opposite anomalies with those of pure El Niño years in general; negative geopotential height anomalies over the Bay of Bengal extend to India (Fig. 10a, b) at 500 hPa and the anomalous moisture flux around 20°N is westward from the southern part of China to the northern part of India (Fig. 10c, d). The moisture

budget shows the moisture convergence (divergence) anomaly of 3.0×10^7 (1.4×10^7) kg s^{-1} based on the NCEP/NCAR (ECMWF) data. The different signs of the two datasets are due to the lack of 2 years, 1954 and 1955, in the composites by use of the ECMWF data, suggesting no systematic anomalies over the plateau in the pure La Niña years. The surface temperature anomalies are not significant either over the plateau (Fig. 10e, f). We note that the negative geopotential height anomalies over the Bay of Bengal in the mid-troposphere strengthen the Indian winter monsoon. Thus, the surface temperature over India decreases.

4 Mechanism

Since only IOD shows significant influences on the early winter TSC, we here focus on possible mechanisms linking IOD with TSC. The composites for differences between the pure positive and negative IOD years based on NCEP/NCAR data are shown only. We note that composites based

**Fig. 9** As in Fig. 7, but for pure El Niño years
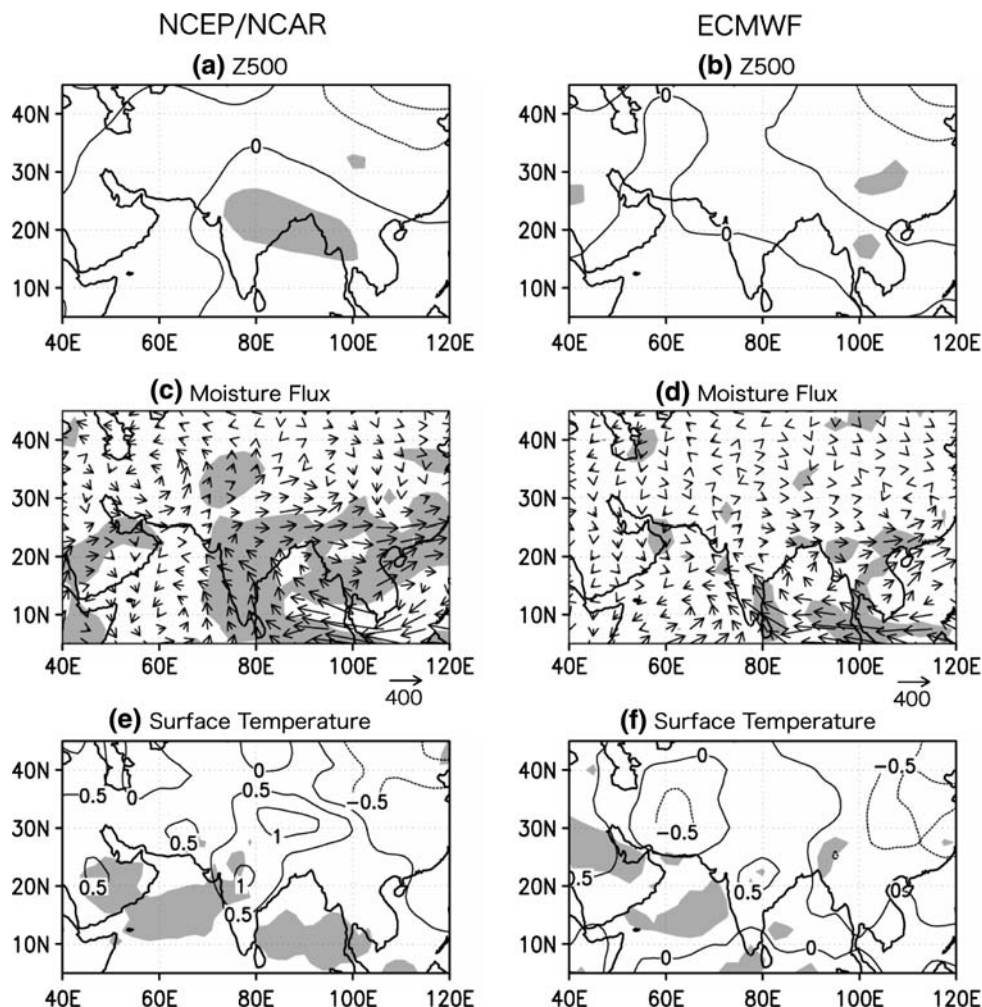
on ECMWF data are similar with those based on NCEP/NCAR data.

The composite of geopotential height anomalies at 250 hPa reveals alternate positive-negative anomaly pattern in the mid-latitude, which is indicative of stationary Rossby waves along the South Asian wave guide in IOD years (Fig. 11, lower panel). The vertical structure of those waves is equivalent barotropic as partly seen in the upper panel of Fig. 11. The negative (positive) geopotential height anomalies north of India in the pure positive (negative) IOD years change the circulation around the Tibetan Plateau and increase (decrease) the snowfall there.

To examine the Rossby waves more in detail, the wave-activity flux $\bar{W}$ is calculated by use of the method developed by Takaya and Nakamura (2001). In the pure positive IOD years (Fig. 12), the wave energies (fluxes) propagate eastward from the Atlantic Ocean to the Mediterranean/Sahara region, change southeastward to the Arabian peninsula, then turn northeastward toward the northern part of India and converge mostly there. The convergence helps to maintain the negative geopotential height anomaly north of

India. Based on the monsoon-desert mechanism introduced by Rodwell and Hoskins (1996), Guan and Yamagata (2003) have discussed the teleconnection between 1994 IOD and circulation changes over the Mediterranean/Sahara region in summer (June–August), claiming that positive IOD can cause convergence anomalies there in the upper troposphere. The warming due to the consequent downdraft of dry air steadily perturbs the mid-latitude westerly and causes Rossby waves carrying air mass eastward along the South Asian wave guide. The anomalous convergence over the Mediterranean/Sahara region can also be seen in the early winter due to the strong divergence over the western/central Indian Ocean in the upper troposphere (Fig. 13, lower panel) caused by SSTA related to IOD (Fig. 13, upper panel). Therefore, the Rossby waves along the wave guide in the early winter of pure IOD years may be caused by the IOD-related convection anomalies over the tropical Indian Ocean. As demonstrated by Sardeshmukh and Hoskins (1988; Fig. 7a, therein) using a vorticity model, a divergence center over the tropical western Indian Ocean can directly generate the

Fig. 10 As in Fig. 7, but for pure La Niña years
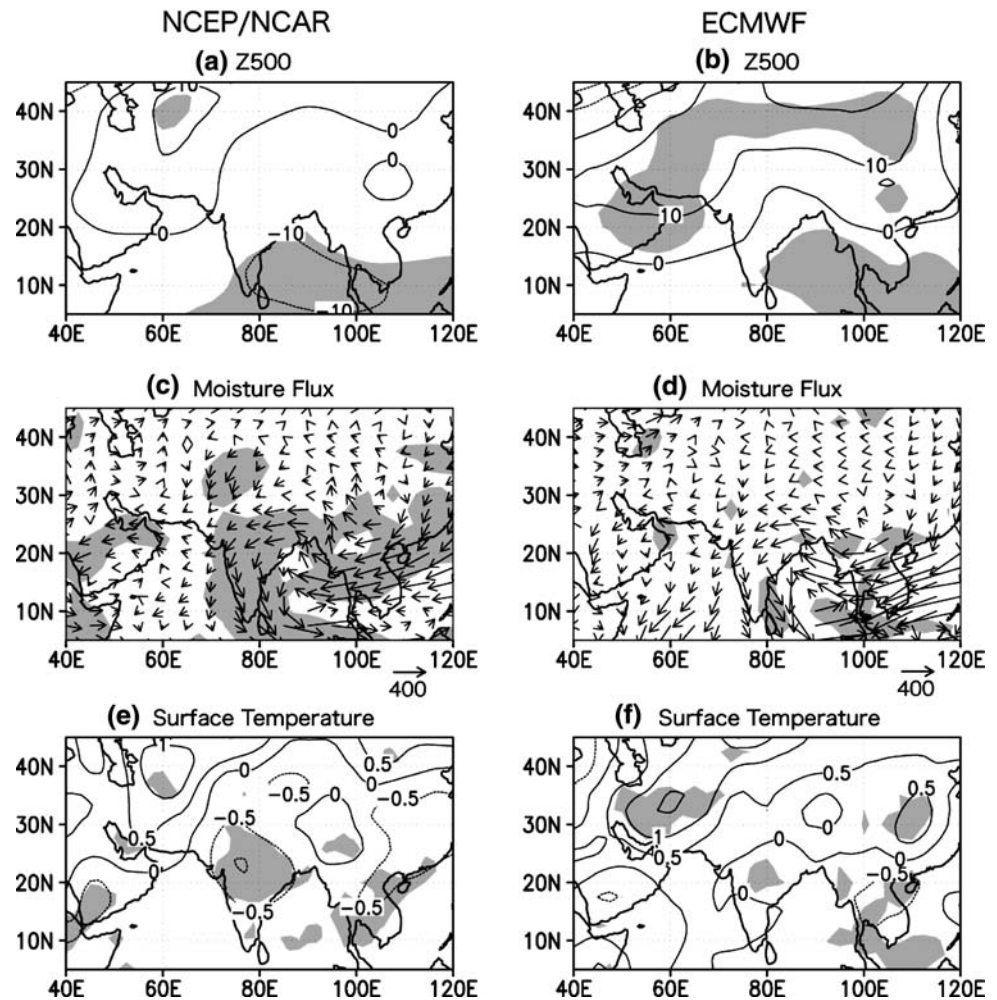
mid-latitude stationary Rossby waves with negative geopotential height anomalies north of India. More recently, Barlow et al. (2007) put an additional deep diabatic heating over the eastern Indian Ocean around the eastern pole of IOD in winter. A westward long Rossby wave response in the mid-latitude and a suppressed precipitation over the South Asia were generated in an AGCM. Further studies using an AGCM to confirm this mechanism are under way.

5 Conclusion and discussion

Using reanalysis data and snow cover data derived from satellite observations, respective influences of IOD and ENSO on the early winter TSC are investigated.

Results show that the early winter TSC has a significant positive partial correlation with IOD. In the pure positive IOD years, the negative (positive) geopotential height anomalies north of India are associated with anomalous warm and humid southwesterlies entering the plateau after rounding cyclonically from the Bay of Bengal. This leads to an increased moisture supply, more precipitation, lower surface temperature, and more snow cover over the Tibetan Plateau. The geopotential height anomalies north of India are related to the stationary Rossby wave along the South Asian wave guide. The waves are equivalent barotropic and can be generated by the downdraft over the Mediterranean/Sahara region. The downdraft is caused by the anomalous divergence over the western/central Indian Ocean due to the IOD-related diabatic heating. We also note that the anomalous divergence over the western/central Indian Ocean (Fig. 13, lower panel) may also be responsible to the generation of the stationary Rossby waves in the mid-latitude as a direct response to the heating in the tropics (Sardeshmukh and Hoskins 1988; Barlow et al. 2007).

In the pure ENSO years, however, the anomalies including surface temperature and moisture flux are not significant over the plateau, indicating negligible influences of ENSO on the early winter TSC. Further analyses using the partial correlation technique that excludes the effects of IOD show insignificant influences of ENSO on TSC in the subsequent spring and early summer either (Fig. 5, grey

Fig. 11 November–December geopotential height differences (in m) between pure positive and negative IOD years at 500 (*upper panel*) and 250 (*lower panel*) hPa based on NCEP/NCAR data. Differences with significance levels at 90% by two-tailed *t* test are shaded
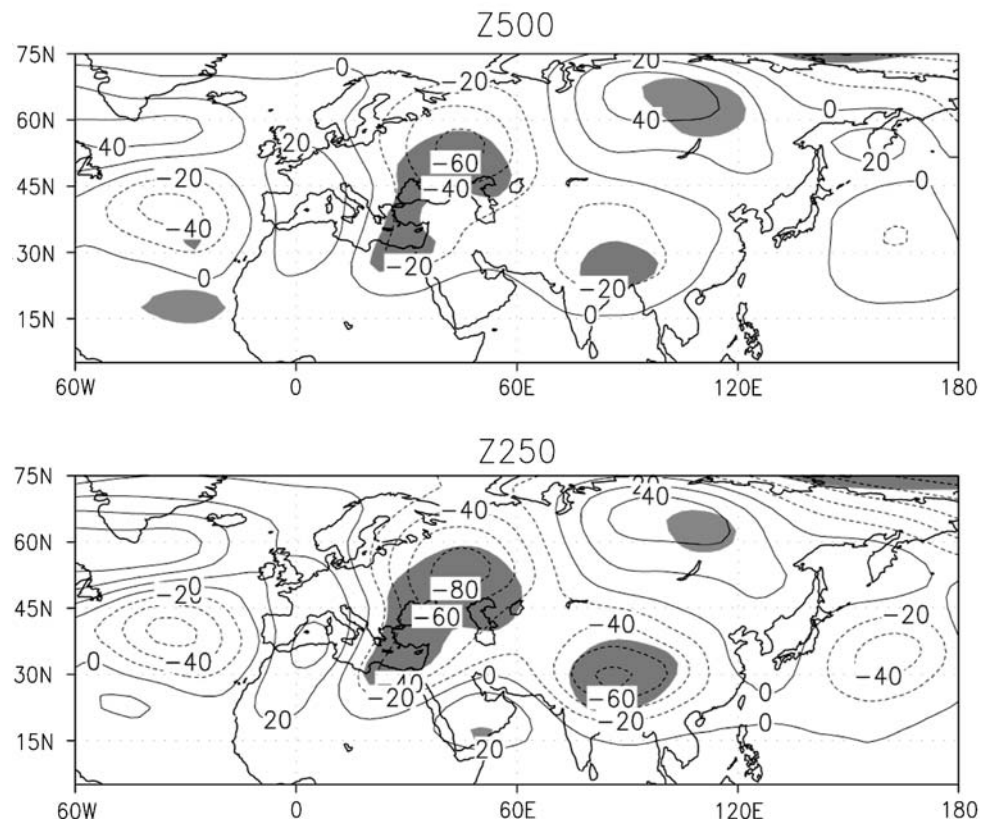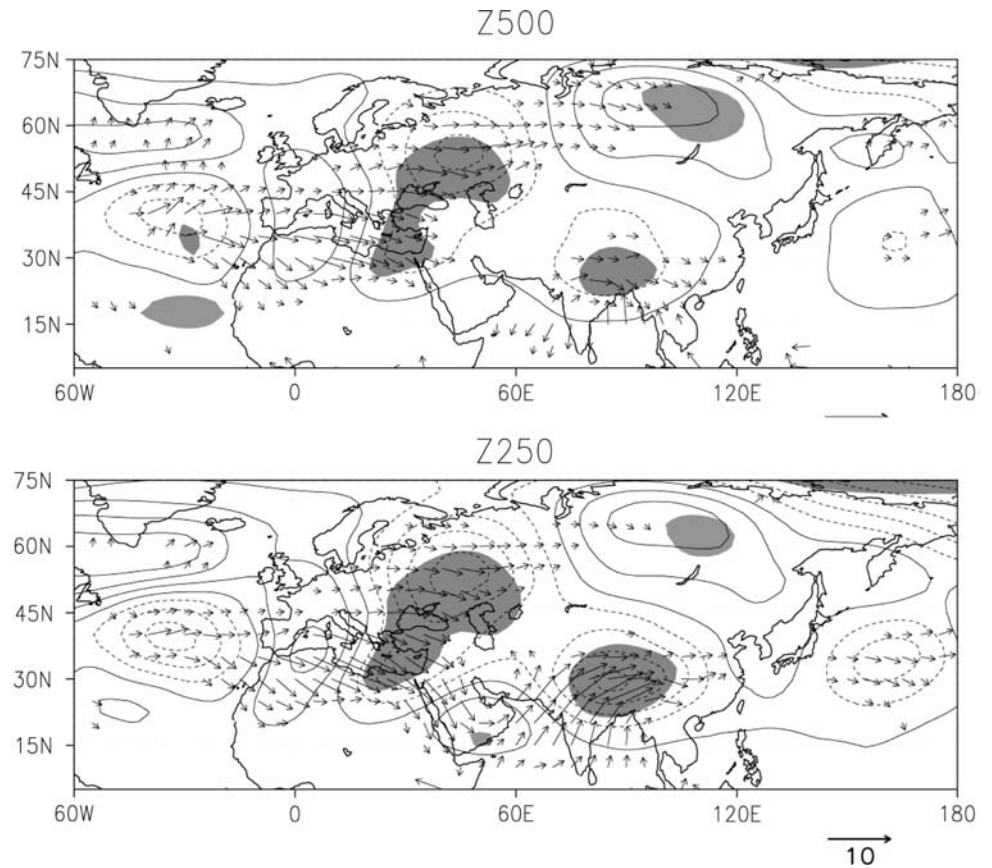

Fig. 12 November–December composites of wave-activity flux (vector, in m² s⁻²) superimposed to geopotential height anomalies (contour, in 20 m) at 500 (*upper panel*) and 250 (*lower panel*) hPa between pure positive and negative IOD years based on NCEP/NCAR data. Differences with significance levels at 90% by two-tailed *t* test are shaded
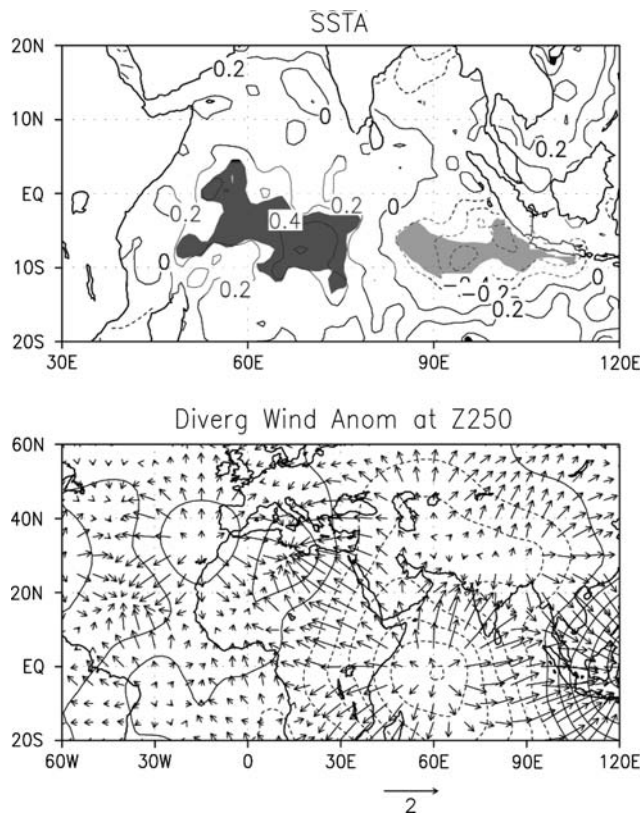
Fig. 13 November–December composites of SSTA (*upper panel*, in °C) and divergent wind anomalies (*lower panel*, vector, in m s^{-1}) superimposed to velocity potential anomalies (*lower panel*, contour, in 0.5 m^2 s^{-1}) at 250 hPa between pure positive and negative IOD years. SSTA with significance levels at 90% by two-tailed *t* test are shaded

bar). However, there is a significant positive partial correlation between TSC in the preceding spring/summer and ENSO at the end of the year. This may be explained by the interactions among the Tibetan snow, Indian summer monsoon and ENSO; more spring/summer Tibetan snow weakens the Indian summer monsoon and the weakened monsoon may trigger or enhance the development of El Niño (Kirtman and Shukla 2000).

Since the sea surface temperature anomalies over the Indian Ocean are different between the pure IOD and pure ENSO years, the corresponding convective anomalies are quite different (Ashok et al. 2003). Pure positive IOD events cause the well-organized anomalous Walker circulation with an ascending branch over the warm western pole and a descending branch over the cold eastern one. These convective anomalies cause steady divergence anomalies at the upper troposphere over the Indian Ocean and excite Rossby waves along the South Asian wave guide. In contrast, the convective anomalies in the pure El Niño years are less organized with case-dependent ascending and descending branches above the basin-wide warm SSTA, and thus generate atmospheric

circulation anomalies different with those in pure positive IOD years.

The present study illustrates the positive influences of IOD on TSC in the early winter. These snow anomalies can last long and favor further snow accumulation by the lower ground temperature. This is why DMI keeps statistically significant positive partial correlation with TSC from the early winter to the subsequent early summer (Fig. 5, dark bar). Therefore IOD can preserve its footprints via the Tibetan snow anomalies and influence the subsequent spring and summer climate even after its disappearance. This result is complementary to the study of Kripalani et al. (2005, 2007), in which they showed the delayed influences of IOD on the summer precipitation in East Asia (i.e., China, Korea, and Japan) three to four seasons after the peak time of IOD and suggested the delayed effects carried by the memory of continental snow anomalies induced by IOD over Eastern Eurasia. Hence, to further understand the role of IOD on the global climate, we need to study more about the prolonged effects of IOD through both ocean and continental surface processes. Efforts to simulate these processes using a coupled general circulation model (CGCM) will be useful to improve our seasonal prediction.

We know that spring/early summer snow anomalies over the plateau can modify the atmospheric circulation over South Asia and the Indian Ocean basin as mentioned in the introduction. This may influence IOD consequently. Actually, the spring/early summer TSC has a negative correlation with DMI in the same year at a 90% significance level (Fig. 5, dark bar). Taking into account the influences of IOD on TSC, this suggests a possible IOD–TSC interaction; positive IOD causes larger TSC in the following spring/early summer and the enlarged spring/early summer TSC triggers the occurrence of negative IOD in the following summer/autumn. This IOD–TSC interaction, if exists, will introduce a biennial nature of IOD. More studies are necessary to confirm this interesting IOD–TSC interaction.

References

Alexander MA, Lau NC, Scott JD (2004) Broadening the atmospheric bridge paradigm: ENSO teleconnections to the tropical west Pacific-Indian Oceans over the seasonal cycle and to the North Pacific in summer. In: Wang C, Xie SP, Carton JA (eds) Earth's

climate: the ocean-atmosphere interaction. Geophysical Monograph, vol 147. AGU, Washington DC, pp 85–103

Ashok K, Guan Z, Yamagata T (2003) A look at the relationship between the ENSO and the Indian Ocean Dipole. J Meteorol Soc Jpn 81:41–56. doi:10.2151/jmsj.81.41

Blanford HF (1884) On the connection of the Himalayan snowfall with dry winds and seasons of droughts in India. Proc R Soc Lond 37:3–22. doi:10.1098/rspl.1884.0003

Barlow M, Hoell A, Colby F (2007) Examining the wintertime response to tropical convection over the Indian Ocean by modifying convective heating in a full atmospheric model. Geophys Res Lett. doi:10.1029/2007GL030043

Fasullo J (2004) A stratified diagnosis of the Indian Monsoon-Eurasian snow cover relationship. J Clim 17:1110–1122. doi:10.1175/1520-0442(2004)017<1110:ASDOTI>2.0.CO;2

Ferranti L, Molteni F (1999) Ensemble simulations of Eurasian snow-depth anomalies and their influence on summer Asian monsoon. Q J R Meteorol Soc 125:2597–2610. doi:10.1002/qj.49712555913

Guan Z, Yamagata T (2003) The unusual summer of 1994 in East Asia: IOD Teleconnections. Geophys Res Lett. doi:10.1029/2002GL016831

Hahn DJ, Shukla J (1976) An apparent relationship between Eurasian snow cover and Indian monsoon rainfall. J Atmos Sci 33:2461–2462. doi:10.1175/1520-0469(1976)033<2461:AARBES>2.0.CO;2

Kalnay E et al (1996) The NCEP/NCAR 40-year reanalysis project. Bull Am Meteorol Soc 77:437–471. doi:10.1175/1520-0477(1996)077<0437:TNYRP>2.0.CO;2

Kirtman BP, Shukla J (2000) Influence of the Indian summer monsoon on ENSO. Q J R Meteorol Soc 126:213–239

Kripalani RH (2007) A possible mechanism for the delayed impact of the Indian Ocean Dipole Mode on the East Asian Summer Monsoon. APCC [APEC (Asia-Pacific Economic Co-operation) Climate Center] Newsletter, Busan, South Korea, vol 2, No 4, 4–6 December 2007. http://www.apcc21.net

Kripalani RH, Kulkarni A (1999) Climatology and variability of historical Soviet snow depth data: some new perspectives in Snow-Indian Monsoon tele-connections. Clim Dyn 15:475–489. doi:10.1007/s003820050294

Kripalani RH, Kulkarni A, Sabade SS, Khandekor ML (2003) Western Himalayan snow cover and Indian summer monsoon rainfall: a re-examination with INSAT and NCEP/NCAR data. Theor Appl Climatol 74:1–18. doi:10.1007/s00704-002-0699-z

Kripalani RH, Oh JH, Kang JH, Sabade SS, Kulkarni A (2005) Extreme monsoons over East Asian: possible role of Indian Ocean Zonal Mode. Theor Appl Climatol 82:81–94. doi:10.1007/s00704-004-0114-z

Li PJ (1993) Characteristics of snow cover in western China. Acta Geogr Sin 48:505–514

Qin D, Liu S, Li P (2006) Snow cover distribution, variability, and response to climate change in western China. J Clim 19:1820–1833. doi:10.1175/JCLI3694.1

Rayner NA, et al (2003) Global analyses of sea surface temperature, sea ice, and night marine air temperature since the late nineteenth century. J Geophys Res. doi:10.1029/2002JD002670

Rodwell MJ, Hoskins B (1996) Monsoons and the dynamics of deserts. Q J R Meteorol Soc 122:1385–1404. doi:10.1002/qj.49712253408

Saji NH, Goswami BN, Vinayachandran PN, Yamagata T (1999) A dipole mode in the tropical Indian Ocean. Nature 401:360–363

Sardeshmukh P, Hoskins B (1988) The generation of global rotational flow by steady idealized tropical divergence. J Atmos Sci 45:1228–1251. doi:10.1175/1520-0469(1988)045<1228:TGOGRF>2.0.CO;2

Shaman J, Tziperman E (2005) The effect of ENSO on Tibetan Plateau snow depth: a stationary wave teleconnection mechanism and implications for the South Asian monsoons. J Clim 18:2067–2078. doi:10.1175/JCLI3391.1

Shukla J (1984) Predictability of time averages. Part II: The influence of the boundary forcing. In: Burridge DM, Kallen E (eds) Problems and prospects in long and medium range weather forecasting. Springer, Heidelberg, pp 155–206

Shukla J, Mooley DA (1987) Empirical prediction of the summer monsoon rainfall over India. Mon Weather Rev 115:695–703. doi:10.1175/1520-0493(1987)115<0695:EPOTSM>2.0.CO;2

Takaya K, Nakamura H (2001) A formulation of a phase-independent wave-activity flux for stationary and migratory quasigeostrophic eddies on a zonally varying basic flow. J Atmos Sci 58:608–627. doi:10.1175/1520-0469(2001)058<0608:AFOAPI>2.0.CO;2

Walker GT (1910) On the meteorological evidence for supposed changes of climate in India. Mem Indian Meteor 21:1–21

Wu TW, Qian ZA (2003) The relation between the Tibetan winter snow and the Asian summer monsoon and rainfall: an observational investigation. J Clim 16:2038–2051. doi:10.1175/1520-0442(2003)016<2038:TRBTTW>2.0.CO;2

Yamagata T, Behera SK, Luo JJ, Masson S, Jury MR, Rao SA (2004) Coupled ocean-atmosphere variability in the tropical Indian Ocean. In: Wang C, Xie SP, Carton JA (eds) Earth's climate: the ocean–atmosphere interaction, vol 147. Geophysical Monograph. AGU, Washington DC, pp 189–212

Yamagata T, Masumoto Y (1989) A simple ocean-atmosphere coupled model for the origin of a warm El Nino Southern Oscillation event. Phil Trans R Soc Lond 329 A:225–236

Zhang Y, Li T, Wang B (2004) Decadal change of the spring snow depth over the Tibetan Plateau: the associated circulation and influence on the East Asian summer monsoon. J Clim 17:2780–2793. doi:10.1175/1520-0442(2004)017<2780:DCOTSS>2.0.CO;2